

Synergy effect in the photocatalytic degradation of textile dyeing waste water by using microwave combustion synthesized zinc oxide supported activated carbon

P. Suresh · J. Judith Vijaya · L. John Kennedy

Received: 13 August 2014 / Accepted: 17 October 2014 / Published online: 29 October 2014
© Akadémiai Kiadó, Budapest, Hungary 2014

Abstract Zinc oxide nanoparticle supported activated carbon (ZSAC) was successfully prepared using a cost effective microwave irradiation method. The earned UV light sensitive ZSAC composites were characterized using powder X-ray diffraction (XRD), high resolution scanning electron microscopy with energy dispersive X-ray analysis, and X-ray photoelectron spectroscopy. The optical properties of ZSAC composites were investigated using UV–Vis diffuse reflectance spectroscopy and photoluminescence spectroscopy, which exposed prolonged light absorption in UV light region and hold better charge separation capability, respectively as compared to pure ZnO. The photocatalytic activity was tested by the degradation of textile dye waste water (TDW) under UV light irradiation. Chemical oxygen demand of TDW was calibrated before and after the photocatalysis experiment under UV light to evaluate the mineralization of wastewater. The results demonstrated that ZSAC composites showed imposing photocatalytic enrichment over pure ZnO and commercial TiO₂ (Degussa P25). The coordinated blending of the oxygen vacant sites, structural defects of ZnO along with electron transmission capacity and presence of surface oxygen on AC has led to the lasting light absorption, delayed charge recombination, and sustenance, which favor the enrichment of the photocatalytic activity of ZSAC.

Keywords Photocatalytic degradation · ZnO nanoparticles · Activated carbon · Synergy effect

P. Suresh · J. J. Vijaya (✉)
Catalysis and Nanomaterials Research Laboratory, Department of Chemistry, Loyola College,
Chennai 600 034, India
e-mail: jjvijayaloyola@yahoo.co.in; jjvijaya78@gmail.com

L. J. Kennedy
Materials Division, School of Advanced Sciences, VIT University, Chennai Campus,
Chennai 600 048, India

Introduction

The wastewater released from the textile industry contains high chemical oxygen demand (COD) and hardly corresponds to the discharging standards recommended by the Indian pollution control boards [1]. In the past, hydrolysis in a basic medium, chemical processes, membrane filtration, biological treatment and foam flotation [2] were employed to treat the waste water, but did not bear desired result [3]. Among numerous modern treatment processes tested to treat the textile dyeing effluents, heterogeneous photocatalysis turns out as the best, because it is a profitable treatment process [4]. In recent investigations, TiO_2 and ZnO were used extensively as heterogeneous photocatalysts. ZnO nanostructures have created adequate interest, by virtue of its wide band gap (3.30 eV), great exciton binding energy of 60 eV, optical and electronic properties [5]. ZnO was used for the degradation of 4-chlorophenol, rhodamine B, methylene blue, procion blue herd from real textile wastewater and acid black 1 [6–9]. But, due to its limitation factor of high percentage of electron–hole recombination, and practical difficulties, exploration is still going on for ZnO composite material.

Advanced explorations have disclosed that the photocatalytic efficiency of TiO_2 and ZnO increased to a great extent, when it was supported on the activated carbon. The preminent impact of AC would be its high adsorption efficiency, which can assist by enhancing the organic molecules around the catalyst, quicken the pollutant transport process, and as a result enhancing the photocatalytic efficiency. It can also increase the life time of electron–hole pairs and promote the target reactions. The mechanism of the synergistic effect of adsorption by AC and photocatalytic decomposition by TiO_2 and ZnO has been studied in the degradation of considerable number of organic pollutants [10, 11].

In the current work, we focused on the preparation and characterization of pure ZnO and ZnO supported activated carbon (ZSAC) composite catalysts. There are many methods available to impregnate ZnO onto the carbon surface, but solution combustion synthesis is a profitable method for the fabrication of ZnO onto the carbon support. Also, the microwave assisted combustion synthesis is environment friendly, rapid, and cost effective.

The influence of carbon support on ZnO photocatalytic efficiency was investigated from the degradation of textile dyeing waste water under UV light irradiation. The as-prepared novel ZSAC exhibited extended UV light absorption, greater adsorptivity of textile dye and enhanced photocatalytic activity than pure ZnO and commercial TiO_2 (Degussa P25).

Materials and methods

Preparation of ZSAC

Zinc oxide supported activated carbon was prepared by using the subsequent procedure. The carbon support for the fixing of ZnO nanomaterials was prepared from the agricultural wastes. The rice husk obtained from public rice factory was

chemically activated at 800 °C using chemical the activating agents, such as HF and KOH. The carbon support (AC), thus, manufactured had a large surface area (446.44 m²/g), pore volume (0.021 cm³/g) and average pore diameter (01.89 nm).

Zinc nitrate hexahydrate and urea of analar grade (Merck, India) were used as the starting for the fabrication of ZSAC. Stoichiometric measure of zinc nitrate hexahydrate and urea were dissolved independently in 10 ml of distilled water. Liquefied urea was combined with aqueous zinc nitrate hexahydrate solution. To this concoction, 1 g of AC was added, and stirred for 5 h. The mixture attained was heated in a microwave (2.45 GHz, 750 W) for 10 min. The output was washed with distilled water, and dried in an hot air oven at 100 °C for 1 h and is designated as ZSAC. Five samples of ZSAC were prepared with varying the ZnO loading from 10 to 50 %. The samples were named as ZSAC1, ZSAC2, ZSAC3, ZSAC4 and ZSAC5. The pure ZnO was also prepared by using the same procedure, without adding carbon support for comparison reason.

Characterization of ZSAC

The crystallinity of AC and ZSAC were analyzed by using a Philips X³pert X-ray diffractometer for 2 theta values ranging from 10 to 80° using CuK_α radiation at $\lambda = 1.540 \text{ \AA}$. A Perkin–Elmer infrared spectrometer was utilized for analyzing the functional groups on the surface of the samples in the spectral range of 4,000–400 cm⁻¹. Morphological analysis and energy dispersive X-ray analysis were done by using a Jeol JSM6360 high resolution scanning electron microscope. X-ray photoelectron spectroscopy (XPS, Make: Kratos analytical (UK), Model: Axis ultra) with a monochromatic MgK_α X-ray source. The XPS curves of C-1s, O-1s and Zn-2P were deconvoluted into convenient number of peaks by using Gaussian fitting. The band gap energy of the samples was estimated from the data obtained from Cary100 UV–Visible spectrophotometer. The photoluminescence properties of the nanostructures were recorded by using a Varian Cary Eclipse Fluorescence spectrophotometer. The specific surface area and porosity was evaluated from the surface area and porosity analyzer (ASAP 2020 V3.00H, Micromeritics Instrument Corp., Norcross, GA).

Photocatalytic reactor setup and the degradation procedure

The photocatalytic degradation of textile dyeing waste water (TDW) obtained from the dyeing industry, Tiruppur, Tamilnadu, India was carried out in a multi lamp photocatalytic reactor. The reactor contains the low pressure mercury lamps (8/8 W) emitting 365 nm UV radiation, which is sufficient for the photocatalytic degradation of TDW. The TDW were taken in glass reactor tubes, which can hold 100 ml of the dye solution. The procedure to study the photocatalytic degradation study is of the following sequence. Textile dyeing waste water is characterized by prominent absorption peaks at 220, 257, 306, 398, 473 and 583 nm. The mineralization of TDW was obtained by measuring the decrease of COD of the waste water. The COD of TDW was determined before and after the photocatalytic treatment with a standard dichromate method using COD digester. The known

initial COD of the TDW was taken and known weights of ZSAC or pure ZnO/TiO₂ (Degussa P25) were added. It was kept in the dark for 12 h to reach the adsorption equilibrium, and the resultant COD was calculated. This solution was taken in the photocatalytic reactor and UV irradiation was supplied for 2 h. At regular intervals of 20 min, equal aliquots were removed from the reactor tube, centrifuged and the COD was estimated to measure the TDW degradation. The percentage of COD removal was calculated from the formula,

$$\% \text{ removal of COD (mg/L)} = (\text{initial COD} - \text{final COD}/\text{initial COD}) \times 100$$

The Indian pollution control board standard has fixed that the let-out TDW from the textile industries into the river bodies must have only 250 mg/L COD, and hence the photocatalytic degradation of TDW was carried out using ZSAC to degrade it to 250 mg/L COD.

Results and discussions

X-ray diffraction analysis

The AC and ZSAC samples were analyzed by X-ray diffraction (XRD) in the range of 2θ between 10° and 80° . The corresponding XRD pattern of the AC, ZSAC (1–5) are shown in Fig. 1. The existence of peaks at 2θ angles 31.58° , 34.41° , 36.21° , 47.56° , 56.58° , 63.03° , 66.39° , 68.19° , and 69.21° accounted for the presence ZnO and they correspond to (100), (002), (101), (102), (110), (103) (200), (112) and (201) planes (JCPDS card No. 89- wurtzite hexagonal phase). These planes of ZnO are then linked with d-spacing standards of 2.80, 2.59, 2.46, 1.90, 1.62, 1.47, 1.40, 1.37, and 1.35 Å, appropriately.

In AC, two peaks at 2θ angles of 23° and 29° correspond to the presence of silica in the carbon matrix. AC showed a broad peak at 2θ angle of 22° , which accounts for the presence of mineral SiO₂, and a small peak at 2θ angle of 44° was obtained for (010) plane of graphitic structure [12]. The presence of a portion of silica was also identified for all the ZSAC samples by the EDX analysis. This implies that silica, which is one of the main constituent of the precursor is not expelled from the carbon matrix even at the high temperature that is reached during microwave irradiation. The intensity of the graphitic peak at 44° decreased drastically in ZSAC, which may be due to the ZnO nanostructures formation on the AC matrix. The existence of graphite in AC will play a decisive role in the growth mechanism of ZSAC.

The crystallite size of ZSAC samples was estimated by using the Scherrer equation [13].

$$L = \frac{0.9\lambda}{\beta \cos \theta}$$

Here, λ is X-ray wavelength, θ is Bragg diffraction angle and β is peak width at full width half maximum. Among the peaks, we selected the strongest peak (101) at

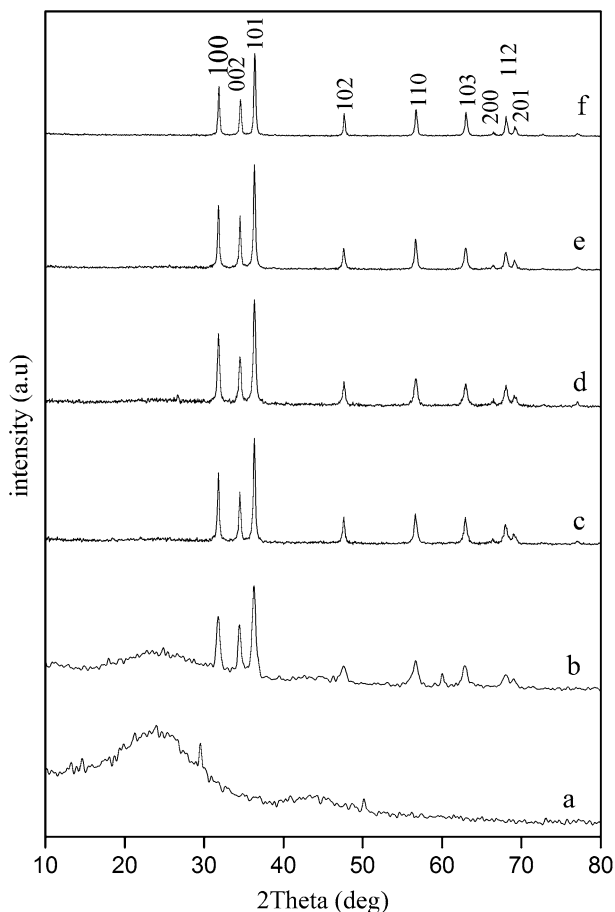


Fig. 1 XRD patterns of *a* AC, *b* ZSAC1, *c* ZSAC2, *d* ZSAC3, *e* ZSAC4, and *f* ZSAC5

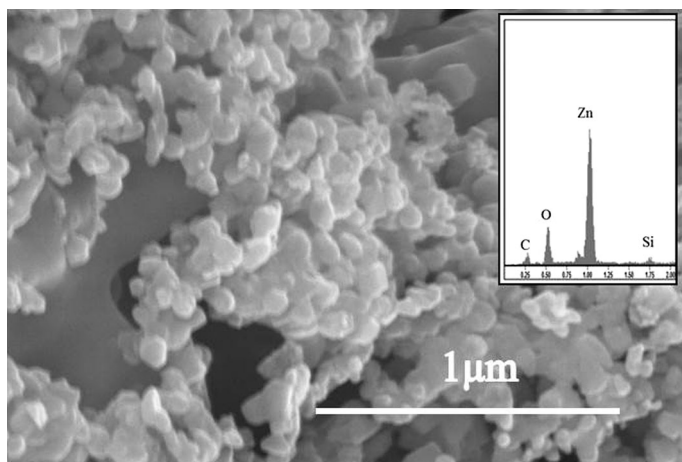
$2\theta = 36.21^\circ$ to calculate the crystallite size. The estimated crystallite sizes of ZSAC (1–5) samples are shown in (Table 1). It was observed that crystallite size increases with an increase in ZnO loading.

Morphology of pure ZnO and ZSAC

HR-SEM micrographs of pure ZSAC5 are shown in Fig. 2. HR-SEM images show the presence of agglomerated irregular spherical shaped nanoparticles. Since the samples are prepared by combustion synthesis in a microwave burning, independent, homogenous growth of nanostructures are not feasible. The production of nanoparticles cannot be guarded in a combustion synthesis, due to the liberation of high amount of heat, and this always produces particles with differing sizes. As a consequence, the HR-SEM image of ZSAC5 ranges from 25 to 110 nm.

Table 1 Crystallite size, band gap, PL emission peaks and PL regions of ZSAC (1–5)

Sample	Crystallite size (nm) $2\theta = 36.21^\circ$ Plane (101)	Band gap (eV)	PL emission peaks (nm)	Emission region
ZSAC1	19.71	3.24	433, 485 and 536	Blue-green
ZSAC2	24.89	3.23	432, 485 and 537	Blue-green
ZSAC3	27.11	3.21	432, 485 and 538	Blue-green
ZSAC4	31.21	3.20	433, 485 and 536	Blue-green
ZSAC5	34.18	3.16	433, 485 and 536	Blue-green

**Fig. 2** HR-SEM image and *inset* EDX analysis of ZSAC5

The elemental analysis of ZSAC5 sample was characterized by X-ray energy dispersive spectrometer (EDX). In Fig. 2, the inset depicts the EDX patterns of the ZSAC5 sample. On careful investigation, the sample contains the elements of C, O, Si and Zn. The existence of silica in the sample indicates that the silica is not fully removed from the carbon support even at the high temperature reached in microwave heating.

XPS Analysis

Fig. 3a shows the full-range XPS spectra of the ZSAC5 revealing the Zn, C and O peak. Fig. 3b shows the profile of the Zn 2p electron, a doublet of the Zn 2p_{3/2} and Zn 2p_{1/2} peaks from the Zn²⁺ states, which are at 1,044 and 1,022.5 eV, respectively, as well as their corresponding shake-up resonances at 1,023 and 1,047 eV. These peaks confirm the presence of Zn²⁺ in ZSAC [14]. But there is a shift of the 2P_{3/2} peak to higher energy, which is ascribed to the incorporation of ZnO into the carbon matrix [15]. It also results in the charge transfer from Zn²⁺ to the carbon matrix.

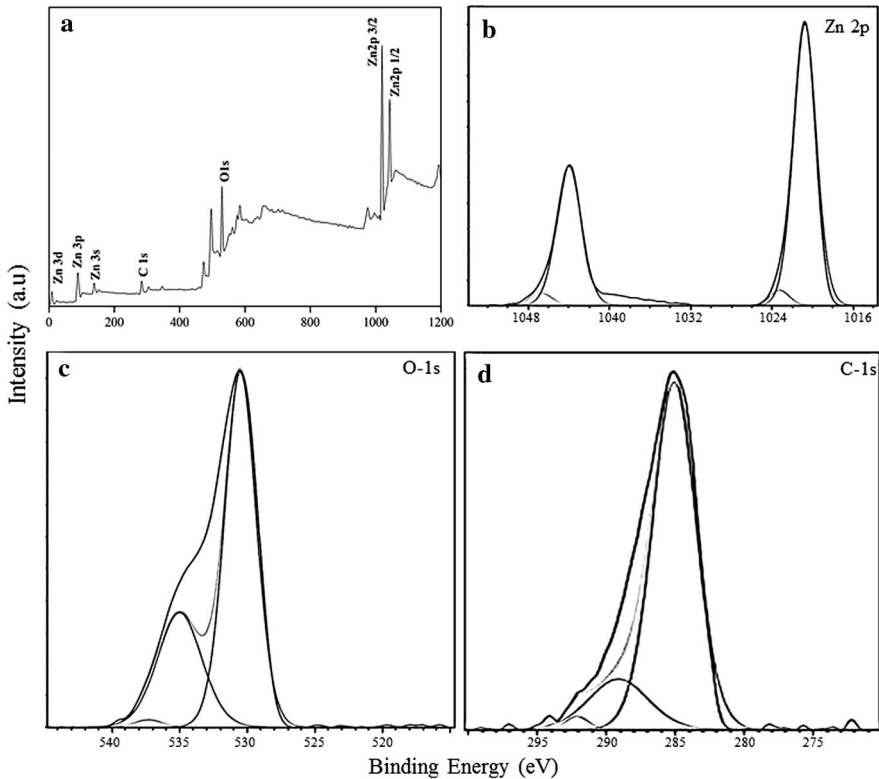


Fig. 3 XPS spectra of ZSAC5 **a** wide spectra, **b** Zn 2p, **c** O-1s and **d** C-1s

Fig. 3c shows the O 1s peaks, which can be deconvoluted into three components centered at about 527–534, 531–540 and 535–539 eV. The major peak at 530.5 eV attributed to the O_2^- ions on the wurtzite structure of the hexagonal Zn^{2+} ion cluster, the O_2^- ions are enclosed by zinc atoms with the absolute accompaniment of adjacent neighbor O_2^- ions [16]. It also implies the adsorbed oxygen on the vacancy sites of ZnO samples, and it is associated with the O^- sub-lattice and further it corresponds to the carbonyl oxygen atoms [17]. The shoulder peak at 535 eV corresponds to the oxygen atoms in the carboxyl groups and minor peak 537 eV to the contribution of absorbed water [18].

The high resolution XPS spectra of the C 1s region is displayed in Fig. 3d, and the peak at 284.9 eV corresponds to the sp^2 carbon bonding in graphitic carbon. The peak at 289 eV is ascribed to carbonyl, quinone, lactone, or ester groups [19]. Besides, an extra peak at high binding energy at about 292.1 eV is associated with $\pi \rightarrow \pi^*$ transitions [20]. It can also be inferred to C=C–O surface group [21]. Thus, the existence of ZnO on the carbon matrix is confirmed by XPS studies.

Optical studies

Diffuse reflectance spectroscopy (DRS) studies

The reflectance spectra were analyzed using a modified Kubelka–Munk function $F(R)$ [22], estimated from the following equation,

$$F(R) = (1 - R)^2/2R$$

$F(R)$ is the Kubelka–Munk function, where R is the reflectance. A graph was plotted between $[F(R)h\nu]^2$ and $h\nu$, and the intercept value obtained corresponds to the band gap energy. The band gaps were evaluated by using the modified Kubelka–Munk function as shown in Fig. 4. The calculated bandgap for pure ZnO and ZSAC (1–5) are shown in (Table 1). The ZSAC samples show smaller band gap when compared with the pure ZnO. This red shift in the band gap for ZSAC could be due to the quantum confinement experienced by the well dispersed ZnO on the carbon matrix, thus leading to lower crystallite size, which is in accordance with XRD results [23]. This effect is likely due to the chemical defects or vacancies present in the intergranular regions generating new energy level to reduce the band gap energy [24]. The diffuse reflectance spectra results clearly show that the ZSAC samples are probable photocatalysts, which can perform efficiently under UV radiation.

Photoluminescence studies

The photoluminescence (PL) spectra of ZSAC (1–5) and pure ZnO samples taken at room temperature employing the excitation wavelength of 325 nm are shown in Fig. 5. The PL peaks and corresponding PL regions are shown in (Table 1). ZSAC samples show an intense PL peak at around 432 nm (2.87 eV) and four broad peaks at 459 nm (2.70 eV), 486 nm (2.55 eV), 525 nm (2.36 eV), and 538 nm (2.30 eV), whereas the pure ZnO show a strong peak at 424 nm (2.92 eV), and four broad peaks at 459 nm (2.70 eV), 486 nm (2.55 eV), 504 nm (2.46 eV), and 536 nm (2.31 eV). The PL intensity of pure ZnO is higher than that of ZSAC (1–5) this indicates that in pure ZnO the radiative recombination is higher, whereas ZSAC (1–5) exhibits higher electron–hole separation, thus enabling it to perform as good photocatalyst.

The blue emission peak (B) around 425 nm is probably by the virtue of two defect levels, either transition from Zn_i to the valence band or transition from the base of the conduction band (CB) to interstitial oxygen (O_i) level [25]. The peak at 459 nm is from the transition between a shallow donor (Zn_i) and deep acceptor (V) [26].

The PL spectra also display the emission bands at 486 and 504 nm in the green region of visible range. The green luminescence mechanism of ZnO still has major difference of opinion, but is commonly designated as the deep-trap-mediated emission [27]. The green light emission can be traced to an oxygen vacancy (VO) [28].

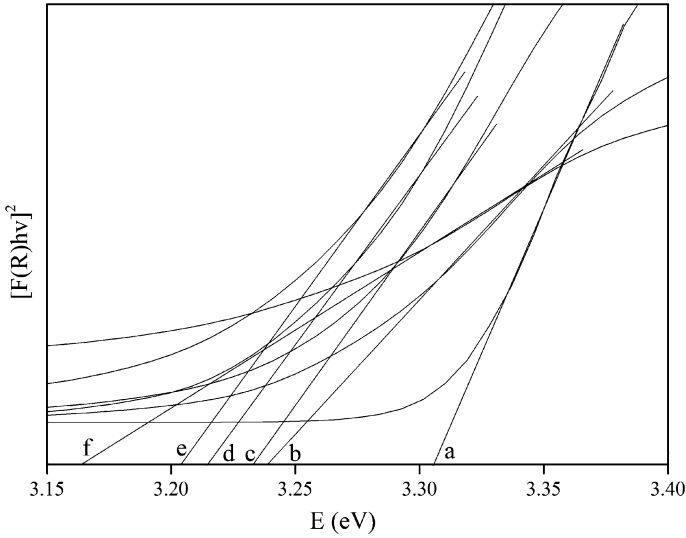


Fig. 4 Diffuse reflectance spectra of *a* pure ZnO, *b* ZSAC1, *c* ZSAC2, *d* ZSAC3, *e* ZSAC4, and *f* ZSAC5

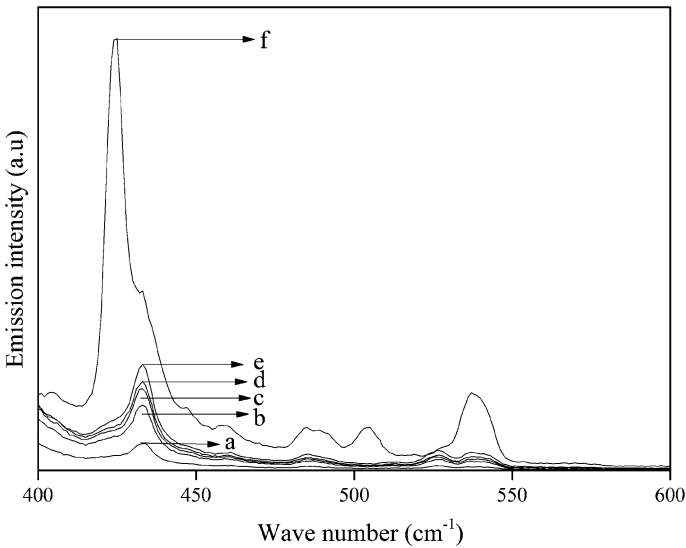


Fig. 5 Room temperature PL spectra of *a* ZSAC1, *b* ZSAC2, *c* ZSAC3, *d* ZSAC4, *e* ZSAC5, and *f* pure ZnO

The presence of green emission around 504 and 536 nm, which confirms the singly ionized oxygen vacancy in ZnO, results from the recombination of a photo generated hole with the single ionized charge state of this defect. The intensity of the green emission peak enormously decreased with increased ZnO loading on the

carbon matrix. This can be accounted for the increased density of surface defect states because of dopant and reduced crystallites size.

Due to the microwave synthesis of ZnO nano structures, structural distortion could have been taken place in the crystal structure. This structural irregularity in ZnO give rise to the intra band gap or the energy levels between the valence and conduction band, and they give rise to the defect emissions. The intra bands are formed, due to the fast evaporation, partial oxidation and rapid crystallization that happen during the microwave heating. These PL peaks distinctly manifest that these bands are not because of the band gap emission, but, they are the consequence of structural defects, such as, oxygen vacancies. The oxygen vacancies on the surface of ZnO samples would favor the O₂ adsorption, and consecutive production of O₂ radical groups, which brings about the oxidation of organic materials [29]. Thus, ZSAC samples with structural defects and oxygen vacancies on their surface would be the potential photocatalysts for the degradation of textile effluents.

Photocatalytic activity

An initial study of the photocatalytic degradation of TDW (1,150 mg/L COD) with ZSAC (1–5) catalysts is carried out and their photocatalytic ability is determined from their COD removal efficiency of the TDW under UV light irradiation. COD removal confirms the destruction of the organic materials in the TDW and the color reduction [14]. The percentage of COD removal obtained for ZSAC (1–5) samples are, 38.4, 45.2, 54.6, 69.1, 78.5 and 90.2 % for 120 min irradiation. The ZSAC5 catalyst was found to be the most efficient one. Hence, ZSAC5 is studied for the various experimental parameters and its photo degradability efficiency is tested with pure ZnO.

A pilot study of COD removal of TDW using AC, ZSAC5 and pure ZnO was carried out. The photocatalytic efficiency of ZnO and AC is lower than that of ZSAC5. The COD removal efficiency is exceptionally intensified in ZSAC5, due to the carbon support. AC as a support can act as dominant electron transmission site, since it exhibits enormous electrical conductivity, and large electron storage capacity, as a result of high specific surface area. AC as support discharged two important roles as an acceptor and transporter of propagated electrons of ZnO and emphatically contained the charge recombination [30]. Besides, due to the well-founded synergy between AC and ZnO nanoparticles, the flow of propagated electrons among the AC and conduction band of ZnO is increased. ZnO is a superior electron contributor, and carbon materials are comparably able electron recipients, the synergistic effect between these constituents adequately reduce the charge recombination. The interblend of the oxygen vacant sites, structural defects of ZnO along with electron transmission capacity and presence of surface oxygen on AC lead to lasting light absorption, delayed charge recombination, and sustenance, which favor the enrichment of the photocatalytic activity of ZSAC5 [31]. The synergy mechanism on the surface of ZSAC5 is illustrated in Fig. 6.

The pH of the medium performs a key part in the photocatalytic degradation mechanism of TDW, since pH alters the generation of hydroxyl radical, a powerful oxidizing agent [32]. To resolve the optimum pH, the pH of the solution was varied

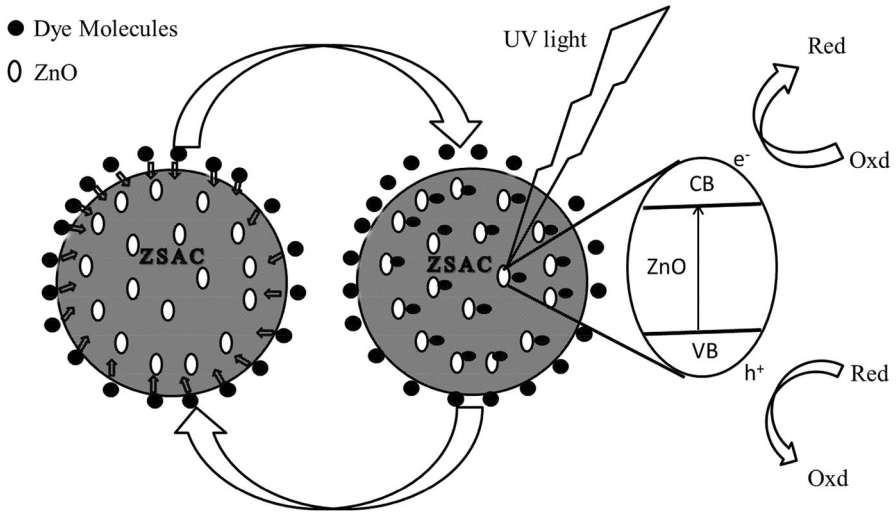


Fig. 6 Synergy mechanism on the surface of ZSAC5

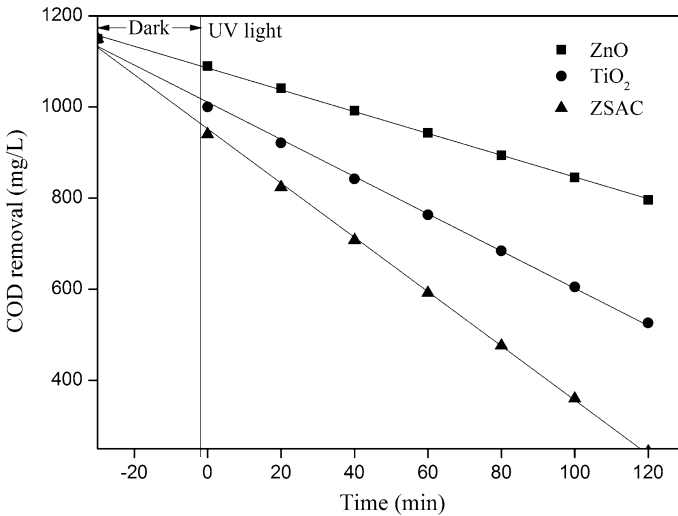


Fig. 7 Kinetic of the TDW photocatalytic degradation by using ZnO, TiO₂, ZSAC5 (Experimental conditions: TDW 1,150 mg/L COD, catalyst dose 1,000 mg/L, pH = 2, λ = 365 nm)

from 2.0 to 12 by adding apt amount of NaOH or H₂SO₄ solutions. It is noticed that the maximum COD removal is achievable in acidic medium, and 100 % COD removal is attained at pH = 2 for ZSAC5. However, ZnO exhibited only 58 % of COD removal at pH = 2. The final pH after photocatalytic treatment was 7.16, which is a proof that the TDW was successfully degraded by the ZSAC and the treated water can be the released into the water bodies. On account of the results obtained, pH = 2 is chosen to be the optimum pH for photodegradation of TDW.

The point of zero charge (pHZPC) of ZnO and ZSAC5 are 7.93, and 8.40, respectively. The surface of the catalyst bears an exclusive positive charge, when the pH of the solution is lower than the pHZPC, it would quicken the adsorption of the negatively charged dyes molecules [33]. Similarly, when the medium turns basic, hydroxide ions are readily adsorbed on the catalyst surface. Ion dipole repulsion between the negatively charged catalyst surface and the negative charged dye molecules is feasible at pH higher than the pHZPC [34]. This is the purpose why TDW is displaying diminished photocatalytic degradation at higher alkalinity.

A kinetic study of the photocatalytic degradation of TDW for ZnO, TiO₂ (Degussa P25) and ZSAC5 was also carried out. The optimized parameters used for the kinetic study are $t = 120$ min, concentration = $1,150 \text{ mg l}^{-1}$ COD, photocatalyst dose = 1.0 g L^{-1} , light intensity = 365 nm and pH = 2. To obtain the kinetics of the photocatalytic degradation, the COD removal versus irradiation time is plotted, which displays the formation of straight lines and indicate the zero-order reaction (Fig. 7). The zeroth order reaction infers that the rate is independent of the reactant concentration, i.e., the extent of dye molecule reacted is proportional to the time. The surface of the catalyst reaches wide amount of coverage by the TDW molecules, and the surface is entirely saturated by the TDW molecules. Thus the rate of the reaction does not depend anymore on the degree of coverage [35]. Mansouri et al. [36] revealed the zeroth order kinetics in the treatment of aqueous organics in the presence of TiO₂, Guerra et al. [30] declared the zeroth order kinetics in the degradation of reactive dyes in the presence of ZnO, and Foletto et al., [37] displayed zeroth order kinetics under sunlight using ZnAl₂O₄. The rate constant for ZnO, TiO₂ (Degussa P25) and ZSAC5 were 2.45, 3.95 and 05.80 ($\text{mL}^{-1}\text{S}^{-1}$). The rate of photocatalytic degradation of ZSAC5 is double than that of pure ZnO and higher than that of TiO₂ (Degussa P25). Activated carbon with a wide surface area, high porosity and various functional groups favours the preferential absorption of TDW on its surface and pores. As a consequence, the TDW molecules are further shifted to ZnO surface, and degraded at a faster rate. The synergy effect between the carbon support and ZnO is responsible for the enhancement in the photocatalytic efficiency of ZSAC5.

Conclusion

In summary, ZnO nanoparticles supported activated carbon (ZSAC) was successfully synthesized through microwave assisted combustion synthesis with simple inorganic salts as raw materials. The XRD and XPS results confirm the presence of ZnO on the carbon support. The uniform loading of ZnO nanoparticles on the carbon surface is revealed by HR-SEM images. The band gaps of the ZSAC samples are in the range of 3.30–3.16 eV. ZSAC samples were used for the photocatalytic degradation studies of TDW. Due to the synergetic effect, ZSAC5 efficiency is higher than the pure ZnO, TiO₂ (Degussa P25) in effective and faster degradation of TDW.

Acknowledgments The authors duly acknowledge the encouragement and financial support rendered by the Salesians of Don Bosco, Dimapur Province, Nagaland, North East India.

References

1. Pholosi A, Ofomaja AE, Naidoo EB (2013) Effect of chemical extractants on the biosorptive properties of pine cone powder: influence on lead (II) removal mechanism. *J Saudi Chem Soc* 17:77–86
2. Barka N, Qourzal S, Assabane A, Nounah A, Ait-Ichou Y (2011) Removal of Reactive Yellow 84 from aqueous solutions by adsorption onto hydroxyapatite. *J Saudi Chem Soc* 15:263–267
3. Lodha B, Chaudhari S (2007) Optimization of Fenton-biological treatment scheme for the treatment of aqueous dye solutions. *J Hazard Mater* 148:459–466
4. Lucas MS, Peres JA (2006) Decolorization of the azo dye reactive black 5 by fenton and photo-fenton oxidation. *Dyes Pigm* 71:236–244
5. Singh AK, Multani SS, Patil SB (2011) ZnO nanorods and nanopolypods synthesized using microwave assisted wet chemical and thermal evaporation method. *Indian J Pure Appl Phys* 49:270–276
6. Pozan GS, Kambur A (2014) Significant enhancement of photocatalytic activity over bifunctional ZnO–TiO₂ catalysts for 4-chlorophenol degradation. *Chemosphere* 105:152–159
7. Shi L, Liang L, Ma J, Meng Y, Zhong S, Wang F, Sun J (2014) Highly efficient visible light-driven Ag/AgBr/ZnO composite photocatalyst for degrading Rhodamine B. *Ceram Int* 40:3495–3502
8. Saravanan R, Karthikeyan S, Gupta VK, Sekaran G, Narayanan V, Stephen A (2013) Enhanced photocatalytic activity of ZnO/CuO nanocomposite for the degradation of textile dye on visible light illumination. *Mater Sci Eng C* 33:91–98
9. Bansal P, Sud D (2011) Photodegradation of commercial dye, procion blue herd from real textile wastewater using nanocatalysts. *Desalination* 267:244–249
10. Matos J, Laine J, Herrmann JM, Uzcategui D, Brito JL (2007) Influence of activated carbon upon titania on aqueous photocatalytic consecutive runs of phenol photodegradation. *Appl Catal B* 70:461–469
11. Lim TT, Yap PS, Srinivasan M, Fane AG (2011) TiO₂/AC composites for synergistic adsorption-photocatalysis processes: present challenges and further developments for water treatment and reclamation. *Crit Rev Environ Sci Technol* 41:1173–1230
12. Sanjaya B, Kalya JR, Srinivasarao S (2010) Rapid growth of nanotubes and nanorods of würtzite ZnO through microwave-irradiation of a metalorganic complex of zinc and a surfactant in solution. *Bull Mater Sci* 33:89–95
13. Cullity BD (1978) Elements of X-ray diffraction. Addison-Wesley Publication Company, Massachusetts
14. Ahmad M, Ahmed E, Hong ZL, Jiao XL, Abbas T, Khalid NR (2013) Enhancement in visible light-responsive photocatalytic activity by embedding Cu-doped ZnO nanoparticles on multi-walled carbon nanotubes. *Appl Surf Sci* 285:702–712
15. Wu C (2014) Facile one-step synthesis of N-doped ZnO micro polyhedrons for efficient photocatalytic degradation of formaldehyde under visible-light irradiation. *Appl Surf Sci*. doi:[10.1016/j.apsusc.04.217](https://doi.org/10.1016/j.apsusc.04.217)
16. Zhu Q, Xie C, Li H, Yang Q (2014) Comparative study of ZnO nanorod array and nanoparticle film in photoelectric response and charge storage. *J Alloy Compd* 585:267–276
17. Machocki A, Ioannides T, Stasinska B, Gac W, Avgouropoulos G, Delimaris D, Grzegorzczak W, Pasieczna S (2004) Manganese–lanthanum oxides modified with silver for the catalytic combustion of methane. *J Catal* 227:282–296
18. Chiang Y, Lee C, Lee H (2007) Surface chemistry of polyacrylonitrile- and rayon-based activated carbon fibers after post-heat treatment. *Mater Chem Phys* 101:199–210
19. Castilla CM, Ramon MVL, Marin FC (2000) Changes in surface chemistry of activated carbons by wet oxidation. *Carbon* 38:1995–2001
20. Okpalugo TIT, Papakonstantinou P, Murphy H, McLaughlin J, Brown NMD (2005) High resolution XPS characterization of chemical functionalized MWCNTs and SWCNTs. *Carbon* 43:153–161

21. Lee WH, Kim SJ, Lee WJ, Lee JG, Haddon RC, Reucroft PJ (2001) X-ray photoelectron spectroscopy studies of surface modified single-walled carbon nanotube materials. *Appl Surf Sci* 181:121–127
22. Hays J, Reddy KM, Graces NY, Engelhard MH, Shutthanandan V, Luo M, Xu C, Giles NC, Wang C, Thevuthasan S, Punnoose A (2007) Effect of Co-doping on properties of ZnO nanoparticles. *J Phys Condens Matter* 19:266203
23. Sathish M, Viswanathan B, Viswanath RP (2006) Alternate synthetic strategy for the preparation of CdS nanoparticles and its exploitation for water splitting. *Int J Hydrog Energy* 31:891–898
24. Song X, Gao L (2008) Facile synthesis of polycrystalline NiO nanorods assisted by microwave heating. *J Am Ceram Soc* 91:3465–3468
25. Hao YM, Lou SY, Zhou SM, Yuan RJ, Zhu GY, Li N (2012) Structural, optical, and magnetic studies of manganese-doped zinc oxide hierarchical microspheres by self-assembly of nanoparticles. *Nanoscale Res Lett* 7:100
26. Behera D, Acharya BS (2008) Nano-star formation in Al-doped ZnO thin film deposited by dip-dry method and its characterization using atomic force microscopy, electron probe microscopy, photoluminescence and laser Raman spectroscopy. *J Lumin* 128:1577–1586
27. Huang MH, Mao S, Feick H, Yan H, Wu Y, Kind H, Weber E, Russo R, Yang PD (2001) Room-temperature ultraviolet nanowire nanolasers. *Science* 292:1897–1899
28. Yan Z, Ma Y, Wang D, Wang J, Gao Z, Wang L, Yu P, Song T (2008) Impact of annealing on morphology and ferromagnetism of ZnO nanorods. *Appl Phys Lett* 92:081911–081911–081911–081913
29. Liqiang J, Yichun Q, Baiqi W, Shudan L, Baojiang J, Libin Y, Wei F, Honggang F, Jiazhong S (2006) Review of photoluminescence performance of nano-sized semiconductor materials and its relationships with photocatalytic activity. *Sol Energy Mater Sol Cells* 90:1773–1787
30. Guerra WNA, Santos JMT, Araujo LRR (2012) Decolorization and mineralization of reactive dyes by a photocatalytic process using ZnO and UV radiation. *Water Sci Technol* 66:158–164
31. Matos J, Laine J, Herrmann JM (1998) Synergy effect in the photocatalytic degradation of phenol on a suspended mixture of titania and activated carbon. *Appl Catal B* 18:281–291
32. Wang Y (2000) Solar photocatalytic degradation of eight commercial dyes in TiO₂ suspension. *Water Res* 34:990–994
33. Kosmulski M (2009) pH-dependent surface charging and points of zero charge. IV. Update and new approach. *J Colloid Interface Sci* 337:439–448
34. Tang WZ, Huang CP (1995) Photocatalyzed oxidation path ways of 2,4-dichlorophenol by CdS in basic and acidic aqueous solutions. *Water Res* 29:745–756
35. Mendive CB, Bahnemann DW, Blesa MA (2005) Microscopic characterization of the photocatalytic oxidation of oxalic acid adsorbed onto TiO₂ by FTIR-ATR. *Catal Today* 101:237–244
36. Mansouri L, Bousselmi L, Ghrabi A (2007) Degradation of recalcitrant organic contaminants by solar photocatalysis. *Water Sci Technol* 55:119–125
37. Foletto EL, Battiston S, Simoes JM, Bassaco MM, Pereira LSF, Flores EMM, Muller EI (2012) Synthesis of ZnAl₂O₄ nanoparticles by different routes and the effect of its pore size on the photocatalytic process. *Microporous Mesoporous Mater* 163:29–33